AEROSERVOELASTIC ROBUST MODEL DEVELOPMENT FROM FLIGHT DATA

Martin J. Brenner
NASA Dryden Flight Research Center
Edwards, California, USA 93523-0273
Email: martin.brenner@dfrc.nasa.gov

Keywords: *aeroservoelastic, uncertainty modeling, robust identification, wavelet filtering*

Abstract

Uncertainty modeling is a critical element in the estimation of robust stability margins for stability boundary prediction and robust flight control system development. There has been a serious deficiency to date in aeroservoelastic data analysis with attention to uncertainty modeling. Uncertainty can be estimated from flight data using both parametric and nonparametric identification techniques. The model validation problem addressed in this paper is to identify aeroservoelastic models with associated uncertainty structures from a limited amount of controlled excitation inputs over an extensive flight envelope. The challenge is to update analytical models from flight data estimates while also deriving non-conservative uncertainty descriptions consistent with the flight data. Transfer function estimates are incorporated in a robust minimax estimation scheme to update models and get error bounds consistent with the data and model structure. Uncertainty estimates derived from the data in this manner provide an appropriate and relevant representation for model development and robust stability analysis. The method incorporates parametric and nonparamteric uncertainty into various uncertainty structures for quantitative measures of robust stability relating to parameter variations and unmodeled dynamics. This model-plus-uncertainty identification procedure is applied to aeroservoelastic flight data from the NASA Dryden Flight Research Center F-18 Systems Research Aircraft (F-18 SRA).

1 Introduction

Aeroservoelastic systems comprise interactions of generally multi-input multi-output sampled-data control feedback with actuation dynamics coupled with aeroelasticity. Highly augmented closed-loop flight test data require extra care in distinguishing system component dynamics. Discrimination of source and response effects for proper understanding of issues in causality may be problematic. Flight test verification of an aeroservoelastic model can also have difficulty in discerning the individual subsystem dynamics because of inaccessible parameters or inadequate sensing for system identification procedures. For instance, aerodynamic parameter identification algorithms for aeroelastic effects may encounter problems with flexibility [1], closed-loop coupling, and transonic nonlinearity.

Model verification over an extensive flight envelope presents more challenges. Test data acquisition is expensive so maneuvers are designed for maximum efficiency and data quality. A verification method is desired which accurately and efficiently includes identification of critical parameters, addresses mismodeling and unmodeled dynamics, deals with test condition and system variability, and derives data-consistent parametric and nonparametric uncertainty descriptions. Parametric uncertainty is generally caused by mismodeling of system properties, off-nominal test conditions, and model over-simplifications. Nonparametric uncertainty often relates to unmodeled dynamics and exogenous inputs, and requires weaker assumptions on the identified system.

With such apparent complications in mind, this paper takes the approach that estimation of aeroservoelastic models must deal directly with uncertainty in model verification. Parameter identification will be applied for model updates from the test data while addressing mismodeling and unmodeled dynamics. Parametric and nonparametric uncertainty

are incorporated to help minimize conservativeness and include both structured and unstructured uncertainty. Non-statistical estimation approaches are preferred to avoid restrictive assumptions, minimize algorithmic complexity, and improve reliability in the form of error bounds. Most importantly, the effectiveness of model-based quantification of uncertainty bounds is appealing for robust control-oriented applications [2, 3, 4].

Set membership identification has been presented in a variety of contexts. Bounded error estimation [5], or bounded data uncertainty [6], characterizes feasible sets of parameters with uncertainty estimates consistent with the data, model structure, and prior information on uncertainty bounds. This last requirement can be in the form of unknown but bounded disturbances [7, 8], constraints on the system impulse response and inputs [9], or assumptions on bounded data perturbations [10].

Two general research directions of set membership estimation are: (1) obtain the exact membership set, and (2) compute a specific optimal estimate in the membership set. The former has suffered from computational complexity and conservatism [7, 11]. An optimal, robust minimax estimate approach is applied in this paper, but the *apriori uncertainty bound is not required*. Minimum upper error bounds are computed with the parameter estimates such that the feasible set is described as a function of the error bounds. Hence, computation of the minimum error bound results in a smallest non-empty feasible set [12].

Transfer functions and modal parameter estimates derived from time-frequency representations have previously been applied to estimate state-space aeroservoelastic models [13, 14]. Morlet wavelet filtering [15, 16, 17] is employed in this paper to update modal parameters as a first step in aeroservoelastic model identification and uncertainty estimation. Standard transfer functions are then employed in the estimation of input-output parameters with associated uncertainty using an optimal minimax procedure. Bounds derived from these estimates define parametric and nonparametric errors which relate to multiplicative and additive uncertainty structures, respectively, for mixed-μ [18, 19] robust stability analyses.

Uncertainty modeling for aeroservoelastic data analysis has not been addressed adequately in the literature. This paper addresses the problem by deriving models with non-conservative uncertainty descriptions consistent with the flight data in a robust control-oriented approach using F-18 Systems Research Aircraft (SRA) [20] data to compare models using multiplicative and additive uncertainty structures.

2 Uncertainty Modeling

The aeroservoelastic open-loop plant model includes rigid body and elastic modes, coupled high-order actuator dynamics, and control surface modal dynamics [21]. Including the aerodynamic lag states, the aeroservoelastic state equations take the following form

$$\begin{aligned} \dot{x} &= Ax + Bu \quad ; \quad u = \delta_d \\ y &= Cx + Du \quad ; \quad x = \lceil \eta_\delta \eta_r \eta_e \dot{\eta}_r \dot{\eta}_e \eta_a \delta \rfloor \end{aligned}$$

consisting of input control surface commands δ_d, actuator states η_δ, rigid body states η_r, flexible mode states η_e, aerodynamic lag states η_a, and control surface displacements δ. Aeroservoelastic plant, P, is therefore represented as the state-space operator. Associated with this time-domain representation is the transfer function, $P(s)$, a function of the complex Laplace variable, s, such that $y = P(s)u$.

$$P(s) \quad = D + C(sI - A)^{-1}B \tag{1}$$

Controller $K(s)$ is modeled similarly, but being a digital implementation of the aircraft control laws, it is modeled as a function of discrete complex variable, z, as $K(z = e^{sT})$ specified by the sampling time T and a zero-order sample-hold at the input of the controller.

A robust characterization of the feedback model incorporates unstructured uncertainty to account for unmodeled dynamics and parameter variations. Unmodeled dynamics are represented with simple cone-bounded transfer functions at the input-output reference locations. Assume the model is suitably scaled with weightings W_1 and W_2 so the uncertainty can be represented by operator $W_1 \Delta W_2$. With uncertainty incorporated into the proper loop reference locations, the robust stability condition is determined by analyzing unity-norm bounded perturbations, $\|\Delta\|_\infty < 1$, with the Small Gain Theorem [19].

Multiplicative uncertainty as shown in figure 1 is used to represent unmodeled dynamics and errors at the feedback output sensors ($w_o = \Delta_o z_o$) and actuator input commands ($w_i = \Delta_i z_i$). Each of Δ_o and Δ_i are diagonal complex perturbations of appropriate output or input dimensions. Performance specifications are in terms of sensor noise attenuation (output response

to output commands) and actuator disturbance rejection (input response to input commands), respectively.

Multiplicative perturbation at the output results in perturbed model $\tilde{P}_o = (I+\Delta_o)P$, and at the input the perturbed model is $\tilde{P}_i = P(I+\Delta_i)$. Necessary and sufficient conditions for unstructured robust stability are then derived from tests on loop sensitivity functions. Unstructured robust stability tests representing these types of uncertainty are described from the complementary sensitivity matrix functions of complex $P(s)$ and $K(s)$, for $\|\Delta_o\|_\infty < 1$ and $\|\Delta_o\|_\infty < 1$.

$$\begin{aligned} \|W_2 T_o W_1\|_\infty \le 1; \qquad & T_o = PK(I+PK)^{-1} \\ \|W_4 T_i W_3\|_\infty \le 1; \qquad & T_i = KP(I+KP)^{-1} \end{aligned} \tag{2}$$

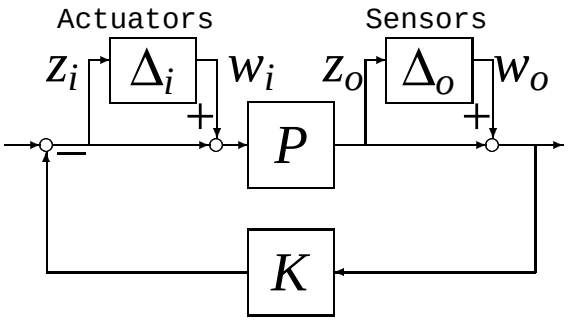

Fig. 1 Aeroservoelastic Model with Input-Output Complex Multiplicative Uncertainty

Another uncertainty characterization of interest in this paper is the additive stable perturbation, Δ_a, for which the perturbed plant is $\tilde{P}_a = P + \Delta_a$ with additive plant errors ($w_a = \Delta_a z_a$) as depicted in figure 2. The corresponding *control action* robust stability test of input response to output disturbances from additive plant errors is imposed by loop shape condition

$$\|W_6 K(I+PK)^{-1} W_5\|_\infty \le \quad 1. \tag{3}$$

A characterization which augments ($w_a = \Delta_a z_a$) with the complex multiplicative uncertainty representation of unmodeled dynamics from figure 1 will also be referred to as the combined structure of additive and multiplicative uncertainty shown in figure 3. Here Δ_a is a full-block complex perturbation since frequency-dependent errors are allowed to enter any of the multi-input-multi-output loops arbitrarily.

The robust stability criteria of (2) vary with the uncertainty description. Uncertainty structure depends on the type of perturbation and how it connects

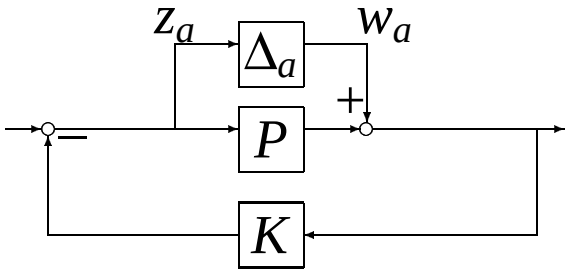

Fig. 2 Model with Additive Plant Uncertainty

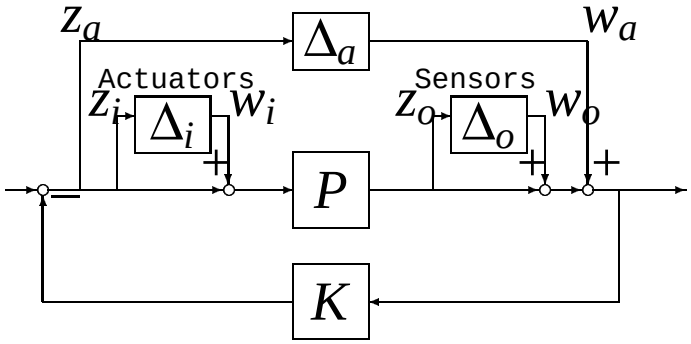

Fig. 3 Additive with Complex Uncertainty

the the nominal system. A *mixed* uncertainty structure consists of (real) parametric and (complex) unmodeled dynamic perturbations and cannot be treated adequately with a simple cone-bounded representation. The structured singular value, μ, is used to reduce conservatism for problems with structured specifications of uncertainty [19, 21]. Robust stability tests of (2) are stated in terms of an upper bound of μ_Δ (noting μ dependence on Δ) at each frequency ω [18].

In this paper, the analysis setup of figure 1 is primarily used as a benchmark for aeroservoelastic stability analysis in the μ framework. In the output-multiplicative parameterization, $\tilde{P}_o = (I+\Delta_o)P$, for example, $y = (I+\Delta_o)Pu$, and

$$z_o = -PK(w_o + z_o) \quad = \quad -(I+PK)^{-1}PKw_o$$

indicate that closed loop stability is guaranteed if $(I+PK)^{-1}PK\Delta_o$ is less than unity. This suggests an interpretation as a multivariable transfer function gain in the sense that $\|T_o\Delta_o\| \le \|T_o\|$ since $\|\Delta_o\| < 1$. To establish a common analysis consistent amongst the various uncertainty structures, while dealing with structured uncertainty in general, the robust stability criteria of (2) are replaced with

$$\mu_{\Delta_o}(W_2 T_o W_1) \le 1 \quad ; \quad \mu_{\Delta_i}(W_4 T_i W_3) \le 1 \tag{4}$$

and the *control action* stability criteria of (3) becomes

$$\mu_{\Delta_a}(W_6K(I+PK)^{-1}W_5) \leq 1, \quad \|\Delta_a\|_\infty < 1. \qquad (5)$$

These conditions imply that for all perturbations matrices, $\{\Delta_o, \Delta_i, \Delta_a\}$, with appropriate structure and satisfying the upper bound constraints, $\|\Delta_o\|_\infty < 1$, $\|\Delta_i\|_\infty < 1$, and $\|\Delta_a\|_\infty < 1$, respectively, the perturbed system is stable. All weights W_i are chosen to scale the auxiliary variables $\{w, z\}$ such that these upper bound constraints are valid. Also, there is a particular perturbation matrix not satisfying the contraints that causes instability, and this is found best from the computational lower bound [18, 19]. Therefore, the μ upper bound plot determines the size of perturbation for which the loop is robustly stable. Lower peaks imply more robust stability.

In the present application, real parameter uncertainty is represented with bounded real perturbations, $[\delta_1, \cdots, \delta_n]$, $|\delta_i|_\infty < 1$, in the aeroservoelastic plant output. A diagonal real-perturbation block is augmented to the complex output perturbation block, Δ_o, to get $w_{ro} = \Delta_{ro} z_{ro}$ from

$$\Delta_r = \begin{bmatrix} \delta_1 & & \\ & \ddots & \\ & & \delta_n \end{bmatrix}; \quad \Delta_{ro} = \begin{bmatrix} \Delta_r & \\ & \Delta_o \end{bmatrix}. \qquad (6)$$

The multiplicative structure from figure 1 is modified with the additional ($w_r = \Delta_r z_r$) as shown in figure 4. Therefore, figure 1 is actually contained in figure 4, but the additional real perturbation block at the output in figure 4 will account for individual modal contributions to the feedback response to the controller. A real-μ analysis augmented with a complex block is a mixed-μ problem. Complex blocks added to real perturbation problems have engineering relevance by accounting for phase uncertainty, besides guaranteeing continuity properties and assisting convergence [18]. The complex blocks, $\{\Delta_o, \Delta_i\}$, for the current problem are also motivated by uncertainty modeling of unmodeled dynamics as a function of the nominal complementary sensitivity transfer functions in (4), and so are retained from figure 1.

Alternatively, the effect of real parametric uncertainty at the plant input or output will be shown to represent an additive uncertainty in the plant transfer function, as in figure 3. In the current analysis, the additive perturbation derived from the plant uncertainty ($w_a = \Delta_a z_a$) will be compared with a consistent real perturbation analysis ($w_r = \Delta_r z_r$) of the associated structured uncertainty of figure 4 for the F-18 SRA aeroservoelastic model.

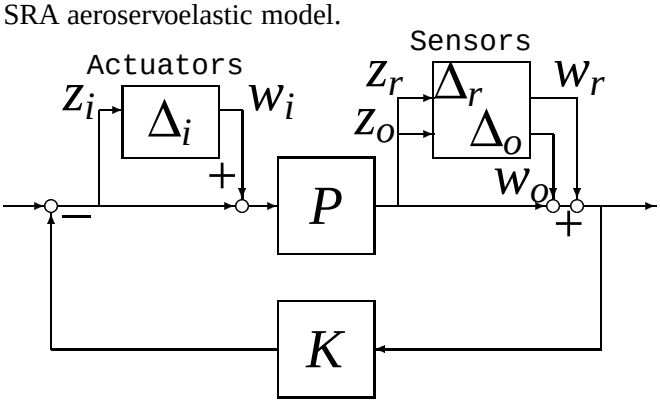

Fig. 4 Input-Complex with Output-Mixed Multiplicative Uncertainty

3 Wavelet-based Modal Estimation

Time-frequency analysis provides a powerful tool for the analysis of nonstationary signals [22, 23, 24]. Signal structure is revealed by quantifying the time-frequency distribution of signal energy as a joint function of time and frequency. Energy density concentrations are revealed as specific areas in the time-frequency plane.

A novel multiresolution wavelet signal processing method is applied to time-frequency analysis of signals by decomposing data into cells with properties of scale and frequency concentrated in time. The cells consist of Gaussian-windowed sinusoidal basis functions, also known as Morlet wavelets, creating a multiscale decomposition in a filter bank structure [24]. Competing requirements of time and frequency resolution, subject to the uncertainty principle [23], is accomplished with a combination of dyadic multiscale decomposition, compact orthogonality, and harmonic wavelet properties [25].

Parameter estimates are derived from time-frequency representations using Morlet wavelet filtering [15, 16]. Morlet filtering is a signal analysis technique which can use time-frequency input information for specification of energy concentrations but does not regard the system as an input-output state-space realization. Morlet wavelets consistute the basis for the energy-density distribution, and assuming the dominant sinusoidal characteristics in sensor responses are modal responses, are then used to estimate the modal parameters. The wavelet basis representation of the

signal is therefore a projection subspace for extraction of modal dynamics.

As a first step in aeroservoelastic model identification and uncertainty estimation, the state-space transfer function plant description of (1) is transformed into real bidiagonal modal form with transformation matrix T.

$$P = \left[\begin{array}{c|c} A & B \\ \hline C & D \end{array}\right] = \left[\begin{array}{c|c} TAT & TB \\ \hline CT & D \end{array}\right] \qquad (7)$$

These two-by-two blocks of complex conjugate roots represent M number of modes, where ζ is the modal damping ratio, ω_n the natural modal frequency, and $\omega_d = \omega_n\sqrt{1-\zeta^2}$ is the damped modal frequency for each mode (ignoring real roots for simplicity here). From this state-coordinate transformation the roots of structural modes are generally simple to discriminate from actuator, rigid body, and aerodynamic lag states. In this paper, parametric errors in modal frequency and damping estimation are not explicitly considered in the uncertainty description, as in previous studies [16, 21]. Justification for this lies in choosing a high confidence factor for allowable estimates to help minimize estimation error [15]. Also, this error will be implicit in the uncertainty model development to be discussed.

Observability of modal dynamics obviously affects identifiability. All available control feedback responses of the aeroservoelastic plant are used to identify modal parameters from each control command maneuver. Numerous reponses become available for estimation of most modes to establish a high degree of confidence from at least one of the responses.

Feedbacks	Control commands
Longitudinal	
pitch rate	symmetric stabilator
normal acceleration	symmetric aileron
Lateral-directional	
roll rate	differential aileron
yaw rate	differential stabilator
lateral acceleration	rudder

Table 1 Feedbacks (left) and controls (right) used for F-18 transfer function and modal parameter estimates.

For the F-18 SRA maneuvers used in this research, table 1 lists the available control commands used to generate the listed feedback signals for modal parameter estimation, and subsequent transfer function estimation for uncertainty analyses. Discrete multisine control commands are the inputs for the aeroservoelastic transfer functions. There are 25 analysis maneuvers in the matrix. Subsets of these correspond to predominantly symmetric or antisymmetric maneuvers, but in reality most modes are excited with either type of input.

4 Minimax Parameter and Uncertainty Estimation

Uncertainty estimation for aeroservoelastic systems depends on a variety of off-nominal factors to consider such as fuel weight, flight condition, control gains, hinge moments, and other aerodynamic effects. The maneuvers used in this research from the F-18 SRA were predominantly flown for the purpose of model verification and update in support of the F-18 Active Aeroelastic Wing Program (AAW) [26]. Flight conditions therefore lie entirely inside the F-18 AAW envelope, which is predominantly transonic and near-transonic. Aerodynamic parameter estimation, loads analysis, and aeroservoelastic model verification were primary flight test objectives for these maneuvers.

System identification with uncertainty modeling requires determination of reliable bounds with the nominal estimates. Interval and bounded-error estimation techniques have pre-defined bounds on the error from apriori knowledge of the system or sensors. This assumption is unacceptable, especially for analysis of aeroservoelastic flight data in the transonic regime, since reliable bounds on the errors do not exist. Most importantly, popular methods for identification are not *model-based*, so the errors are not relevant to the model, but only depend on the data and estimation process itself.

Aeroservoelastic models are often of high order, significant dynamic range, and contain lightly damped modes. Any methods which depend on simultaneous parameter and model order estimation will have complexity problems attempting to discern order from uncertainty. Even for fixed-order estimation, identification of structural parameters with input-output (C and B) parameters is susceptible to non-uniqueness, convergence, and bias problems unless severe assumptions are imposed [3, 14, 27]. Again, these procedures are often based on statistical arguments, and often are not model-based. Stability prediction based on errors between models and aircraft requires uncertainty relative to a model.

4.1 Robust Minimax Parameter Estimation

Robust minimax estimation not only provides the minimum upper bound on the error, but also provides a parameter set compatible with any error upper bound [12]. The problem is stated in terms of error, $\varepsilon(k,\Theta)$, its bound ε, and parameter vector, Θ, given N measured frequency response data, $y(k)$, and model frequency response vector, $\phi(k)$, $k = 1,...,N$.

$$\varepsilon \equiv \|\varepsilon\|_\infty = \max_k |\varepsilon|, \quad \varepsilon(k,\Theta) = y(k) - \phi(k)\Theta \quad (8)$$

Since the minimum upper error bound over frequency, ε, is assumed unknown, it is estimated from the minimax procedure. The minimum value of ε is desired that is consistent with the flight data frequency responses. A solution set is given by

$$\{\hat{\Theta} | \hat{\Theta} = \arg\min_\Theta \max_k |\phi(k)\Theta - y(k)|\} \quad (9)$$

which can be transformed to a differentiable linear programming problem using additional variable, x, subject to constraints, for $k = 1,...,N$.

$$\hat{\Theta} = \arg\min_\Theta (x); \qquad |\phi(k)\Theta - y(k)| \le x$$

It can then be shown that the set of all (x,Θ) consistent with the constraints is a convex unbounded polyhedron, or for any $x \ge \varepsilon$ [12].

$$\Theta \quad = \hat{\Theta} + \Delta\Theta \quad = \hat{\Theta} + \Delta(x) \quad (10)$$

The feasible polytope for (x,Θ) thus contains the exact description of the solution set of $\hat{\Theta}$, including a range of feasible parameters contained in a positive interval $\Delta\Theta$ that satisfies (9) for any $x \ge \varepsilon$. Therefore, the most important property of this approach for uncertainty estimation is that a minimum upper bound on the frequency response error, ε, is found which is compatible with parametric errors, $\Delta\Theta$, so these parametric errors are derived from the value of the *non*-parametric error cost function, $|\varepsilon(k,\Theta)|$.

A seemingly attractive *analytic center* approach to bounded-error estimation was recently proposed [7, 28] to minimize logarithmic average output error.

$$\hat{\Theta} = \arg\min_\Theta \sum_k \log|\phi(k)\Theta - y(k)|$$

This estimator has nice properties in terms of output error minimization, robustness to outliers, and online sequential implementations. However, these properties and error bounds depend on apriori knowledge of noise bounds. This estimator is not chosen because of the necessary noise assumptions and absence of guaranteed parametric error bounds.

4.2 Model Updates and Output-Uncertainty Estimation

Now the procedure for flight data analysis is described in the robust minimax estimation framework. First, the A-matrix of (7) is updated to get estimate, $\hat{A}$, with wavelet modal filtering. Then the column of the $\{B,D\}$-matrices in (7) corresponding to a particular control command input is appropriately scaled by matching the norms of the model and estimated data transfer functions from control command to feedback sensor. These estimates are denoted as $\{\hat{B},\hat{D}\}$. Each element of the model C-matrix corresponds to a modal contribution to the feedback response. Elements of the appropriate row of the model C-matrix corresponding to the feedback response are then chosen for optimization only if they correspond to modal responses within a specified frequency range. Vector $\mathbf{y}$ is the flight data response from a feedback sensor, being a sum of the aircraft modal responses.

Each row of the model C-matrix is expanded as

$$\hat{P} \quad = \quad \left[\begin{array}{ccc|c} \multicolumn{3}{c|}{\hat{A}} & \hat{B} \\ \hline c_1 & 0 & 0 & \\ 0 & \ddots & 0 & \tilde{\hat{D}} \\ 0 & 0 & c_n & \end{array}\right]$$

where $\tilde{\hat{D}}$ is resized from elements of $\hat{D}$ corresponding to diagonalization of a row of C. Arrange the updated model frequency response matrix, $\hat{P}(i\omega_k)$, to form the n-columns (for n states) of matrix Φ, where each column corresponds to a modal frequency response contribution to the total feedback sensor response.

$$\Phi(k,l) = \hat{P}(i\omega_k, l), \quad l = 1,...,n; k = 1,...,N \quad (11)$$

Parameter vector, Θ, is the *multiplier* (nominally $\Theta = [1\cdots1]^T$) on the model response matrix, Φ, to match the flight data response. Absolute transfer function error, ε, is the maximum of the frequency-dependent error vector, $\hat{\varepsilon}$, expressed as follows (compare to (8)).

$$\varepsilon \equiv \|\hat{\varepsilon}\|_\infty = \max|\hat{\varepsilon}|, \quad \hat{\varepsilon} = \mathbf{y} - \Phi\hat{\Theta} = \mathbf{y} - \hat{\mathbf{y}} \quad (12)$$

In light of the robust properties of logarithmic error criteria [28, 29, 30], and the well-known property of Chebyshev estimators being optimal in terms of worst-case parameter error, the objective function is chosen as a log-type Chebyshev estimator.

$$\hat{\Theta} \quad = \quad \arg\min_\Theta \max_\omega \log|\Phi\Theta - \mathbf{y}| \quad (13)$$

There is strong justification for this performance criteria. It has been shown that logarithmic error minimization is superior to absolute error minimization for parametric transfer function estimation, especially for structural systems and high order problems [30]. Properties from (9) still hold in a log-sense since the log function and its inverse (exponential) are monotonic smooth functions of the data. Furthermore, log-based frequency response estimation demonstrates superior performance in closed-loop systems, with mutually correlated signals in feedback, and is robust to noise characteristics and outliers without relying on statistical assumptions [29].

Parametric uncertainty is multiplicative in the real C-matrix values since the identified parameter vector, $\hat{\Theta}$, is a multiplier to the model. This is the optimal nominal estimate. It was also shown that from the identification procedures of (9) or (13), a real positive uncertainty interval $\Delta\Theta$ to this nominal part results from (10). Decomposing the identification problem into these nominal and uncertain parts, an estimate of the real parameter uncertainty becomes (see (12))

$$\begin{aligned} \|\hat{\mathbf{y}}\| + \varepsilon &\equiv \|\Phi\hat{\Theta}\| + \|\Phi \cdot \Delta\Theta\| \\ \Longleftrightarrow \varepsilon &= \|\Phi \cdot \Delta\Theta\| \leq \|\Phi\|\|\Delta\Theta\| \\ \Longrightarrow \Delta\Theta &\approx \frac{\varepsilon.}{\sum_{k=1}^{N} |\Phi_{k,l}|}, \quad l = 1, ..., n \end{aligned} \tag{14}$$

where element-by-element division $(\varepsilon./)$ is implied. In the expression $\Phi \cdot \Delta\Theta$, each uncertain element of $\Delta\Theta$ is weighted by a column sum of Φ. Each element of the positive uncertain vector, $\Delta\Theta$, therefore results from a division by $\sum_k |\Phi_{k,l}|$, a weighting by an inverse absolute column sum (vector 1-norm). This is a decomposition of the absolute total error over frequency, ε, into individual modal contributions in the elements of $\Delta\Theta$. Elements of $\Delta\Theta$ with denominator sums less than a small threshold retain nominal $\hat{\Theta}$ values ($\Delta\Theta(l) = 0$) to avoid numerical problems, but also denote relatively insignificant modal responses (column-sums of $|\Phi|$, see (11)) with no observability.

Note that $\Delta\Theta = \Delta(\varepsilon)$ from the linear programming solution (compare (10) and (14)), so the parametric error is a by-product of the *non*-parametric frequency-dependent global error, $\hat{\varepsilon}$. Also note that the minimum upper bound error, ε, is a constant *additive perturbation bound* over frequency from the relations in (8) and (12). This corresponds to the uncertainty that is added to the nominal estimate, $\hat{\mathbf{y}} = \Phi\hat{\Theta}$, to account for the flight data transfer function, $\mathbf{y}$, from (8). In either case, the non-parametric frequency-dependent error, $\hat{\varepsilon}$, or its more conservative bound, ε, characterizes the additive perturbation error *at each frequency*, $k = 1, ..., N$, in figures 2 and 3.

$$w_a = \Delta_a z_a = \Delta_a |\hat{\varepsilon}_k|, \quad |\hat{\varepsilon}_k| \leq \varepsilon \tag{15}$$

Alternatively, the real-parametric error, $\Delta\Theta$, naturally represents real uncertainty from (6) and figure 4 as a multiplier on the nominal C-matrix. For each output, using element-wise multiplications denoted by $(.*)$, the uncertainty is described by

$$\begin{aligned} C_\Delta \equiv \quad \hat{C} \pm \Delta C &= C. * \hat{\Theta} \pm \Delta C \\ |\Delta C| &\equiv |C. * \Delta\Theta| \\ \|\Delta C\| &\leq \|C. * [\Delta_r \Delta\Theta]\| \end{aligned} \tag{16}$$

where operator Δ_r is the real perturbation defined in (6), $w_r = \Delta_r z_r = \Delta_r \Delta\Theta$, $\|\Delta_r\| < 1$ and therefore $\|\Delta_{ro}\| < 1$ since $\|\Delta_o\| < 1$. Note that real-parametric variation, ΔC, varies equally positively or negatively according to $\|\Delta_r\| < 1$ while $\Delta\Theta$ is a positive range of variation.

It is important to note here that $\Delta\Theta$ therefore serves as both a contribution to the additive error bound (from (14) and (15), allowed to be complex in general to account for phase variations), and also as a multiplicative output real-parametric error in (16), so it is integral to both types of uncertainty descriptions. Despite this relationship, the manner in which the uncertainty is modeled (complex-additive vs. real-multiplicative) determines its structure and will affect the robust stability analysis. Comparisons of both manifestations will be demonstrated next.

5 Aeroservoelastic Data Analysis

Three types of uncertainty structures have been discussed as being relevant to aeroservoelastic uncertainty modeling. They are compared in this section.

- *complex*-multiplicative loop uncertainty (baseline structure, figure 1 with criteria in (4))
- *additive* combined with complex-multiplicative loop uncertainty (combine figures 1 and 2 to get figure 3 with Δ_a in (15))
- *mixed* real-parametric, complex-multiplicative loop uncertainty (figure 4 with (16))

Complex-multiplicative loop uncertainty at the input and output in figure 1 is the baseline analysis. This

baseline structure is augmented with additional perturbation blocks in the additive and mixed analyses. All weights W_i are unity by nature of the perturbation descriptions, maintaining that $\|\Delta\| < 1$ for all perturbations, $w = \Delta z$. All uncertainty analyses operate on models that are updated with the wavelet modal parameter estimates unless stated otherwise. Results are for the F-18 SRA flight condition of Mach 0.9, altitude $5,000$ feet using all three available inputs denoted in table 1 for lateral-directional maneuvers.

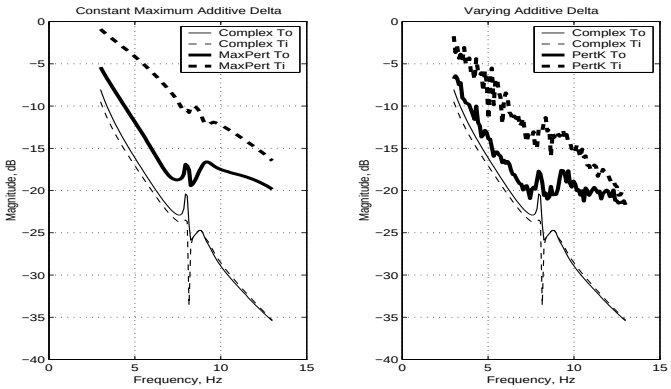

Fig. 5 Complementary sensitiivity μ-analysis.
Left plot: Complex-μ analysis (thin lines, uncertainty structure in figure 1) compared to *upper bound* (ε) additive-μ analysis (thick lines, structure in figure 3)
Right plot: Complex-μ (thin lines) compared to *varying* ($\hat{\varepsilon}_k$) additive-μ analysis (thick lines)

Baseline complex-multiplicative complementary sensitivity μ-analysis results, using a discrete implementation of controller K as mentioned below (1), are compared with additive loop uncertainty at the output (solid) and input (dashed) in figure 5 for the F-18 SRA lateral-directional flight condition. Comparisons between upper-bound additive (ε, left plot) and varying additive ($\hat{\varepsilon}$, right plot) results are presented. Note that the additive results must be at least as large in magnitude as the baseline since *additive also includes complex-multiplicative uncertainty* (figure 3) and therefore includes Δ_a as an additional perturbation to the baseline structure. These plots demonstrate that the estimated minimax error upper-bound is not too conservative compared to the varying error result. Error bounds from the additive minimax analysis of the flight data at this condition are evident as being up to 15dB larger than the baseline result.

Additive and mixed uncertainty are compared with complementary sensitivity complex-multiplicative μ-analysis results in figure 6, again

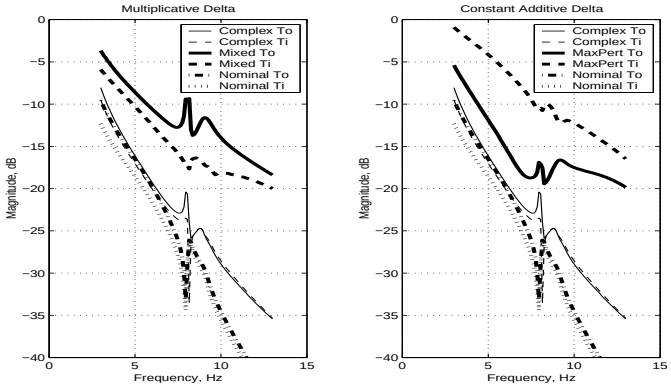

Fig. 6 Complementary sensitiivity μ-analysis.
Left plot: Complex-μ analysis (uncertainty structure in figure 1) compared to mixed-μ analysis (structure in figure 4) and nominal complex-μ analysis
Right plot: Complex-μ analysis compared to additive-μ analysis and nominal complex-μ

for the F-18 SRA lateral-directional flight condition. Also shown in these plots are the *nominal* complex-multiplicative results computed from aeroservoelastic models before any updates from flight-derived parameter estimates were incorporated.

In figure 6 the dominant modes are antisymmetric fuselage first bending (near 8 Hz) and antisymmetric wing first bending (near 9 Hz). Differences in modal pole-zero relationships and modal frequency shifts between the nominal and updated (using $\{\hat{A},\hat{B},\hat{C},\hat{D}\}$) complex-multiplicative results demonstrate the significant effect of parametric updates on the nominal model. As expected, both mixed and additive results are at least as large in magnitude as the baseline. While the output-mixed-μ magnitude is the largest (solid thick line in left plot), and much larger than the output-additive result (solid thick line in right plot), the additive results are reversed in that the input-additive magnitude (dashed thick line in right plot) dominates with values above all the other results. Despite the relationship between the mixed and additive uncertainties ($\Delta\Theta \Longleftrightarrow \varepsilon$, see (14)) the connection is disguised by the manner in which the uniform additive uncertainty, ε from (15), is incorporated in the combined structure of figure 3 compared to the mixed augmentation of $\Delta\Theta$ in (16) and figure 4.

Analysis of numerous flight conditions does not reveal any consistent trends between the mixed and additive results. Quality of models and flight data, and loop structure (longitudinal or lateral-directional) are primary considerations. For example, transonic con-

ditions often exhibit larger uncertainty because of the model sensitivity [21] and the relatively poor quality of flight data from exogenous inputs due to aerodynamic effects. Another source of significant uncertainty can be dynamic modal cross-axis coupling, especially with modes closely-spaced in frequency, between symmetric and antisymmetric modes. Aeroelastic and aeroservoelastic models are often developed with a preferred axis orientation, symmetric or antisymmetric. Cross-axis dynamics will necessarily be revealed as unmodeled dynamics in such a situation.

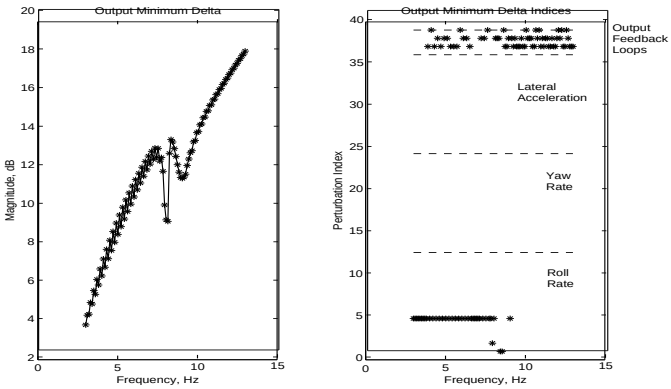

Fig. 7 Mixed uncertainty minimum perturbation-to-instability (left) and index of perturbation (right) corresponding to output mixed-μ analysis.

Lower bounds of μ provide the perturbation, Δ, which causes instability [18] with respect to its structure (see commments below (4)). In the left plot of figure 7, lower bounds are calculated and plotted with line-connected '*'-symbols. Lower values of the minimum perturbation denote the more sensitive frequencies. In the right plot, corresponding indices of the real parameters ($w_r = \Delta_r z_r$, indices 1-37) and complex uncertainty control feedback loops (3 output loops, $w_o = \Delta_o z_o$ with indices 38-40) are marked, also plotted with individual '*'-symbols. This information shows which parametric uncertainties (indices 1-37) or complex-multiplicative loop uncertainties (indices 38-40) in each feedback, at specific frequencies, result in the minimum perturbation-to-instability condition of the left plot. For example, complex-multiplicative uncertainty in all output loops (indices 38-40) is very significant, as seen from a congestion of values at the top of the right plot (3 rows corresponding to indices 38-40 at multiple frequencies). Real parameters, $\Delta\Theta$, contributing to roll rate are the other perturbations important in the instability mechanism, as seen from the row and scatter of points plotted at the bottom. There are no critical real perturbations in the yaw rate (indices 14-25) or lateral acceleration (indices 26-37) loops.

6 Conclusions

Aeroservoelatic model identification with uncertainty is addressed in this paper to present a robust data-oriented procedure for model development. Surface command inputs and control system feedbacks are used as signals in a wavelet-based modal estimation procedure for modal parameter updates. Transfer functions are incorporated in a robust minimax estimation scheme to identify input-output parameters and structured error bounds consistent with the data. Uncertainty estimates derived from the data in this manner provide appropriate and relevant representations for robust stability analysis useful for model validation and control system design. This procedure is an automated, efficient, and reliable approach for analysis of numerous flight data sets for robust stability and model development.

7 References

1. Britt, Robert T., S.B. Jacobsen, and T.D. Arthurs. Aeroservoelastic analysis of the B-2 bomber. *AIAA Journal of Aircraft*, Vol. 37, No. 5, Sep-Oct 2000, pp. 745-752.
2. Andersson, Lennart and A. Rantzer. Frequency-dependent error bounds for uncertain linear models. *IEEE Transactions on Automatic Control*, Vol. 44, No. 11, Nov 1999, pp. 2094-2098.
3. Campbell, Mark E. and S.C.O. Grocott. Parametric uncertainty model for control design and analysis" *IEEE Transactions on Control Systems Technology*, Vol. 7, No. 1, Jan 1999, pp. 85-96.
4. Smith, Roy S. and Mohammed Dahleh, Eds. *The modeling of uncertainty in control systems*. 1992 Santa Barbara Workshop, Springer-Verlag, 1994, pp. 1-75.
5. Milanese, Mario, J. Horton, H. Piet-Lahanier, and É. Walter, Eds. *Bounding approaches to system identification*. Plennum Press, New York, 1996.
6. Sayed, Ali H. and S. Chandrasekaran. Parameter estimation with multiple sources and levels of uncertainties. *IEEE Transactions on Signal Processing*, Vol. 48, No. 1, Mar 2000, pp. 680-692.
7. Bai, Er-Wai, Y. Yue, and R. Tempo. Bounded error parameter estimation: a sequential analytic center approach. *IEEE Transactions on Automatic Control*, Vol. 44, No. 6, June 1999, pp. 1107-1117.

8. Tan, Guojie, C. Wen, and Y.C. Soh. Identification for systems with bounded noise. *IEEE Transactions on Automatic Control*, Vol. 42, No. 7, July 1997, pp. 996-1001.

9. Feng, Xu, C.-F. Lin, and N.P. Coleman. Frequency-domain recursive robust identification. *AIAA Journal of Guidance, Control, and Dynamics*, Vol. 23, No. 5, Sep-Oct 2000, pp. 908-910.

10. Sayed, Ali H. and V.H. Nascimento. Design criteria for uncertain models with structured and unstructured uncertainties. in *Robustness in identification and control*. A. Garulli, A. Tesi, and A. Vicino, Eds., Vol. 245 of Lecture Notes in Control and Information Sciences, pp. 159-173, Springer-Verlag, London, 1999.

11. Rotstein, Héctor, N. Galperin, and P.-O. Gutman. Set membership approach for reducing value sets in the frequency domain. *IEEE Transactions on Automatic Control*, Vol. 43, No. 9, Sep 1998, pp. 1346-1350.

12. Walter, Éric and H. Piet-Lahanier. Recursive robust minimax estimation. *Bounding approaches to system identification*. Milanese, Mario, J. Horton, H. Piet-Lahanier, and É. Walter, Eds., Plennum Press, New York, 1996, pp. 183-197.

13. Brenner, M.J. and E. Feron. Wavelet analysis of F/A-18 aeroelastic and aeroservoelastic flight test data. *AIAA Structures, Structural Dynamics, and Materials Conference*, Kissimmee, FL, Apr 1997, AIAA-97-1216, NASA-TM-4793.

14. Feron, Eric, M. Brenner, J. Paduano, and A. Turevskiy. Time-frequency analysis for transfer function estimation and application to flutter clearance. *AIAA Journal of Guidance, Control, and Dynamics*, Vol. 21, No. 3, May-June 1998, pp. 375-382.

15. Brenner, Marty. Nonstationary dynamics data analysis with wavelet-SVD filtering. *AIAA Structures, Structural Dynamics, and Materials Conference*, Seattle, WA, Apr 2001, AIAA-2001-1586, NASA-TM-2001-210391.

16. Brenner, Marty and R. Lind. Wavelet-processed flight data for robust aeroservoelastic stability margins. *AIAA Journal of Guidance, Control, and Dynamics*, Vol. 21, No. 6, Nov-Dec 1998, pp. 823-829.

17. Ruzzene, M., A. Fasana, L. Garibaldi, and B. Piombo. Natural frequencies and dampings identification using wavelet transform: application to real data. *Mechanical systems and signal processing*, Vol. 11, No. 2, 1997, pp. 207-218.

18. Balas, Gary J., et. al. *μ-analysis and synthesis toolbox*. MUSYN, Inc. and The Mathworks, Inc., 1998i, Chap. 4, pp. 4-1 to 4-86.

19. Zhou, Kemin with John C. Doyle. *Essentials of robust control*, Prentice-Hall, Upper Saddle River, NJ, 1998i, Chaps. 8-10, pp. 129-220.

20. Sitz, Joel R. *F-18 systems aircraft research facility*. NASA-TM-4433, Dec 1992.

21. Lind, Rick and Marty Brenner. *Robust aeroservoelastic stability analysis: Flight test applications*. Series: Advances in Industrial Control, Springer-Verlag, 1999.

22. Hubbard, Barbara B. *The world according to wavelets*. A.K. Peters, Wellesley MA, 1998, Chap. 5, pp. 76-89.

23. Mallat, Stéphane. *A wavelet tour of signal processing*. Academic Press, 1999, Chap. IV, pp. 64-126.

24. Vetterli, Martin and Jelena Kovačević. *Wavelets and subband coding*. Prentice-Hall, Upper Saddle River, NJ, 1995, Chap. 6, pp. 333-368.

25. Le, Dzu K. Application of sampling theorems in wavelet spaces to multiresolution visualization and data segmentation. *SPIE Proceedings of wavelet applications in signal and image processing III*, Vol. 2569, Bellingham, WA, July 1995, pp. 220-233.

26. Pendleton, E., D. Bessette, P. Field, G. Miller, and K. Griffin. Active aeroelastic wing flight research program: Technical program and model analytical development. *AIAA Journal of Aircraft*, Vol. 37, No. 4, July-Aug 2000, pp. 554-561.

27. Zhang, Y.M., R. Kovacevic, and Y.X. Yao. Identification of multivariable interval dynamic model from measurements in frequency domain. *Proceedings of the American Control Conference*, Albuquerque, New Mexico, June 1997.

28. Bai, E.-W. and Y. Yue. Constrained logarithmic least squares in parameter estimation. *IEEE Transactions on Automatic Control*, Vol. 44, No. 1, Jan 1999, pp. 184-186.

29. Guillaume, Patrick, R. Pintelon, and J. Schoukens. Robust parametric transfer function estimation using complex logarithmic frequency response data. *IEEE Transactions on Automatic Control*, Vol. 40, No. 7, July 1995, pp. 1180-1190.

30. Sidman, M.D., F.E. DeAngelis, and G.C. Verghese. Parametric system identification on logarithmic frequency response data. *IEEE Transactions on Automatic Control*, Vol. 36, No. 9, Sep 1991, pp. 1065-1070.